Towards multiphysics 4D particle tracking in microchannels with high-speed light-field microscopy

C. Fort*, M. J. Yamakaitis, P.M. Bardet

Dept. of Mechanical and Aerospace Engineering, The George Washington University, USA
*Corresponding author: cfort@gwu.edu

Keywords: Light-Field Microscopy; 4D Particle Tracking, Microfluidics.

ABSTRACT

This work presents recent progress toward high-resolution, single-camera 4D particle tracking in microfluidic environments using a custom-built Fourier light-field microscope (FIMic). The system captures seven angular views on a single high-speed sensor and enables volumetric particle tracking with sub-micron precision using multi-view reconstruction and Lagrangian tracking. Building on the system originally introduced at the Lisbon Symposium 2024, which demonstrated nearly isotropic particle-localization uncertainty below 0.3 µm, the present work extends the approach through experimentally registered defocused point spread functions (PSFs) and convolutional neural-network-based particle detection. These developments increase the accessible depth of field from approximately 50 µm to more than 160 µm while preserving a 370 µm-wide field of view and high-speed acquisition at 1300 Hz streamed directly to disk. The improved framework is demonstrated in several challenging microfluidic configurations, including pillar wakes, junction flows, and a backward-facing step geometry from the first defocused particle tracking (DPT) challenge introduced this year. These results show that high-speed Fourier light-field microscopy can provide compact, single-camera access to time-resolved 3D flow measurements in optically constrained microchannels. Future work will extend the method beyond seeded-particle velocimetry toward multiphysics measurements involving near-wall transport, biofilms, scalar fields, active microswimmers, and intensity-based reconstructions.

1. Introduction

Accurate measurement of three-dimensional flow in confined microfluidic systems remains challenging because of constraints on spatial resolution, optical access, and system complexity. Conventional techniques such as microscopic PIV (µPIV) (Cierpka & Kähler, 2012; Etminan et al., 2022) often suffer from limited depth resolution, whereas tomographic and stereoscopic configurations require multiple synchronized imagers and careful alignment (Lindken et al., 2006; Giardino et al., 2008; Kim et al., 2011). To address these limitations, we recently introduced a single-camera plenoptic velocimetry system based on Fourier light-field microscopy (FIMic), also referred to

here as plenoptic 3.0, achieving depth resolution on the order of 2 µm and nearly isotropic spatial uncertainty below 0.3 µm in reconstructed particle positions (Fort et al., July 8-11, 2024). This technique eliminates the need for multiple cameras while still enabling volumetric, time-resolved particle tracking using the Shake-the-Box (STB) algorithm. Initial measurements in a cross-junction microchannel demonstrated the ability of the system to resolve complex laminar flows with high fidelity over a $350\ \mu\mathrm{m} \times 50\ \mu\mathrm{m}$ volume using seven elemental views captured by a 6K high-speed imager.

A parallel effort explored an alternative implementation based on retrofitting a commercial inverted microscope with a plenoptic 3.0 adapter to test STB and Richardson-Lucy deconvolution (RLD) approaches in a more accessible configuration (Fort et al., June 26-28, 2025). While the retrofitted microscope enabled validation of scalar-field reconstruction schemes and simplified the experimental setup, the FIMic system remains the highest-resolution implementation available and is used exclusively in the present and future work discussed in this paper.

Unlike most single-camera particle-based microscopy approaches, including confocal scanning µPIV (Park et al., 2004; Oishi et al., 2011), defocused µPIV (Yoon & Kim, 2006; Pereira et al., 2007; Winer et al., 2014; Barnkob et al., 2015; Klinner & Willert, 2022; He et al., 2023), and holographic µPIV (Sheng et al., 2006; Ooms et al., 2009), the present technique captures multiple angular views of the scene and relies primarily on multi-view particle tracking algorithms.

We are now exploiting the complex point spread function (PSF) associated with each angular view to improve the performance of the technique, most notably by increasing the effective depth of field by more than a factor of three. Exploiting the PSF also enables measurements through thicker channel walls, including the configuration used in the first defocused particle tracking (DPT) challenge introduced this year. Here, we detail these developments, present results in microchannel flows, and discuss future work toward multiphysics applications.

2. Methodology

2.1. Experimental apparatus

Figure 1 shows the FIMic instrument deployed as an inverted 4D microscope. The system comprises a custom relay system that conjugates the Fourier plane of a $63\times$ NA 1.0 water-immersion objective with a microlens array (MLA) of 2 mm pitch and 17 mm focal length. The MLA forms a hexagonal array of seven elemental images on a 6K high-speed CMOS sensor (IDT Phoenix Gold) with 3.55 µm pixels, yielding an analytical lateral resolution of 1.75 µm and a depth resolution of 2.56 µm. In the present experiments, the camera sensor is cropped to 1824×1800 pixels. Each elemental image is a disk of 516 pixels, corresponding to 370 µm at a magnification of 4.95, or 0.72 µm/pixel. The system streams directly to a computer hard drive and acquires 10-bit images at

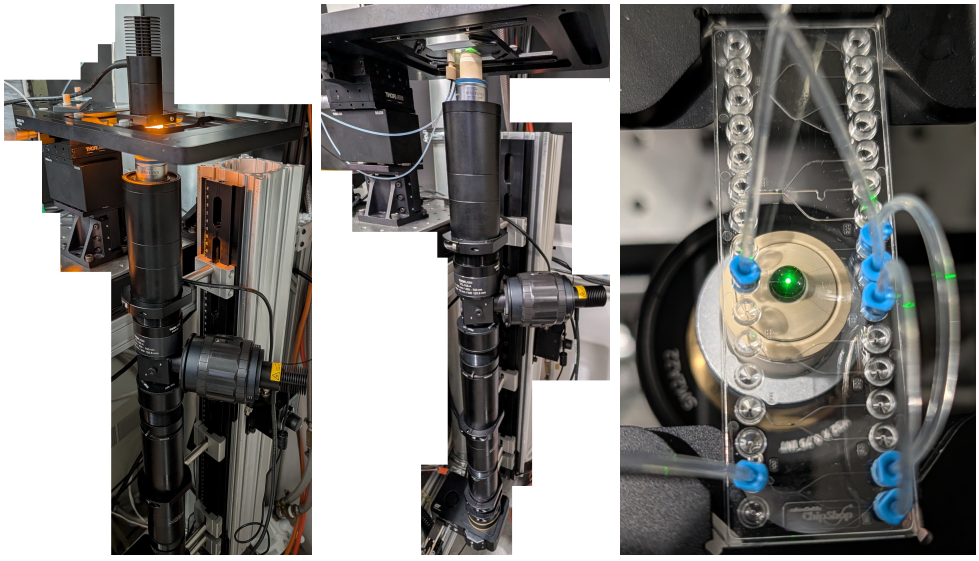


Figure 1. Custom-built light-field imager in calibration mode (left) and active recording mode (center), together with the microfluidic chip studied in Sect. 3.2 (right).

1300 Hz for typical time-resolved runs of 20 s, corresponding to 26,000 frames. An example image containing the seven angular views captured by the single-camera system is shown in Sect. 3.1.

Nile red fluorescent particles (Spherotech FH-2056-2), with diameters between 1.7 and 2.2 µm, are illuminated in epifluorescence configuration using a 530 nm LED in various microchannels. The seeding solution consists of 1 mL of 1.0% w/v particle suspension diluted in 250 mL of distilled water.

In Fort et al. (July 8-11, 2024), the system was calibrated using a grid target with 25 µm spacing, and the seven individual views were extracted and imported as independent cameras into DaVis 10 by LaVision. STB reconstructions yielded thousands of Lagrangian particle trajectories with sub-micron uncertainty in all three directions. In addition to velocity-field measurements, the dataset was processed to assess particle-location uncertainties over sequences of 300-500 frames, revealing nearly isotropic uncertainty distributions across tracked particles. The average uncertainty reported by Davis was below 0.1 µm in the lateral directions and below 0.3 µm in depth. These results provide the baseline from which the present effort expands, although the original reconstructions were limited to a 50 µm depth of field.

2.2. Defocused point spread function

In the improved approach presented here, the elemental views are calibrated using a precision translation stage and a custom dot target with 50 µm spacing and 2 µm apertures. The target is back-illuminated using a 595 nm LED, and the opal substrate acts as a diffuser so that light passing through each aperture is directionally scattered. The diffraction-limited image of each 2 µm aper-

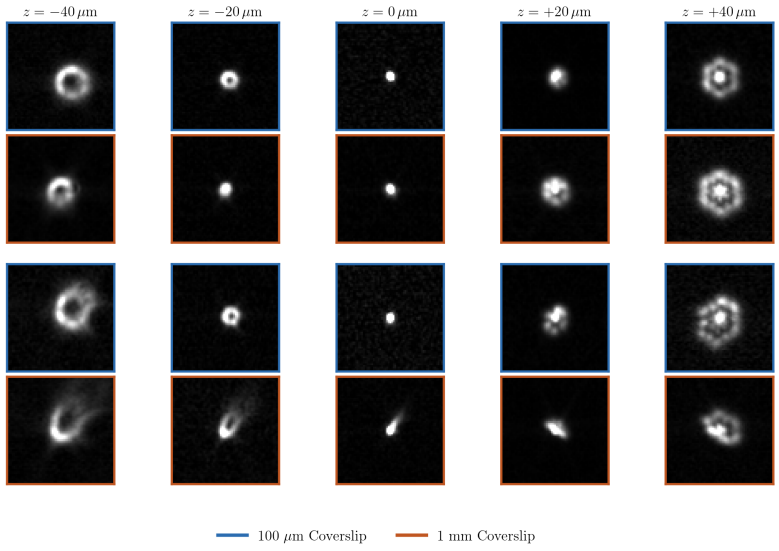


Figure 2. Experimental aperture point spread function (PSFs) for five discrete depths in the central (top two rows) and an off-center (bottom two rows) elemental images for two coverslip thicknesses. Images with the red box are for the 1 mm thick coverslip.

ture is visually equivalent to the PSF generated by fluorescent tracers of the same nominal size. Calibration is performed by scanning the dot grid along the optical axis through the depth of field in 5 µm increments.

Figure 2 shows an aperture image for the central and an off-center view for two coverslip thicknesses: a #1 coverslip (McMaster 1149T13), approximately 145 µm thick, and a standard 1 mm microscope slide. The high numerical aperture of the system, NA = 1.0, has two prominent effects. First, the aperture image defocuses rapidly, with the PSF diameter increasing by approximately 0.6 pixel/µm. Second, the PSF is sensitive to coverslip thickness, an effect that is especially pronounced in the off-center elemental images. The hexagonal pattern of the defocus particle is due to the MLA geometry.

2.3. Particle detection and tracking

Particle detection is performed using a convolutional neural network inspired by Godbersen et al. (2024). Detection is treated independently for each of the seven elemental images, such that each view acts as an independent micro-camera. Standard distorted pinhole camera models are used to map points from 3D world coordinates to 2D image coordinates for each elemental view. A 3D particle position observed in multiple views is then triangulated using standard multi-view methods. The camera model is fitted using the PSF calibration stack described in Sect. 2.2 and subsequently refined using particle images through bundle adjustment, which jointly optimizes the camera parameters and detected particle positions.

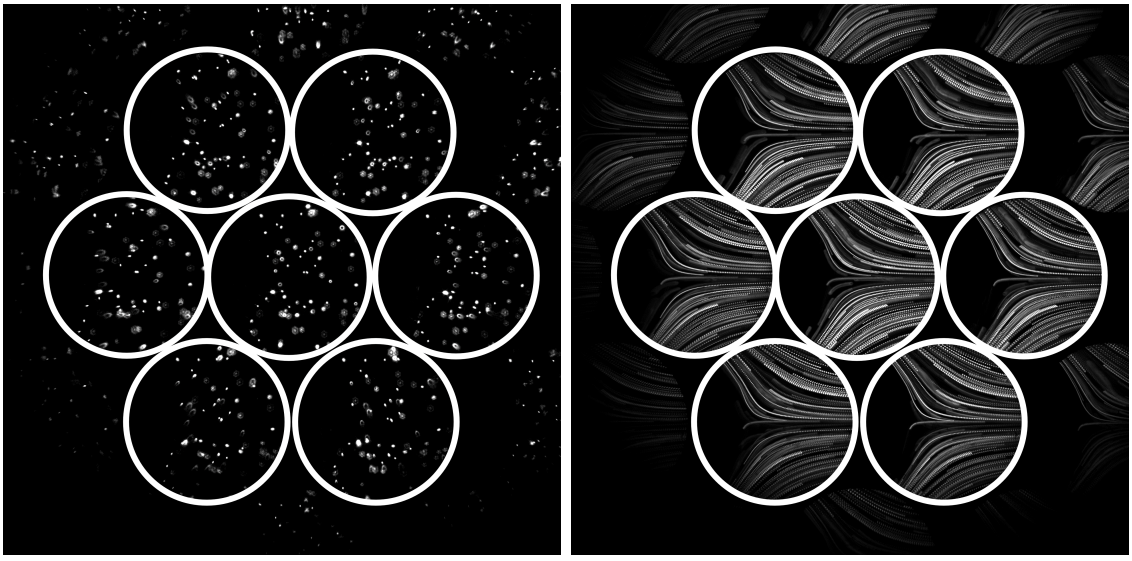


Figure 3. Instantaneous image in the wake of the micropillar (left) and streak image over 130 consecutive frames (right). The background has been subtracted, the contrast has been enhanced, and the seven angular views have been manually highlighted.

In narrow microchannels, the channel walls can occlude particles in some elemental views. Therefore, detections in only three of the seven views are explicitly required to reconstruct a particle position. For each frame, a point cloud of detected particle centers is constructed. Particles are then linked between frames using a nearest-neighbor approach. For tracks with an existing time history, a position predictor is used to support temporal linking. This step is not yet optimal and is currently the factor limiting particle-image density. Several strategies exist in the literature to improve robust linking and refine particle positions, and these will be explored in future work (Ouellette et al., 2006; Schanz et al., 2016; Liang et al., 2021; Mallery et al., 2020; Novara et al., 2023; Mercier et al., 2024; Hao et al., 2024).

3. Results

Results are presented for several microchannel configurations driven by one or two syringe pumps (New Era Infusion One, NE-300). First, we consider two off-the-shelf chips from microfluidic ChipShop, Fluidic 1273 and 1573, made of TOPAS and sealed with a #1 coverslip. The first channel has a $100\,\mu\mathrm{m} \times 9500\,\mu\mathrm{m}$ rectangular cross-section and incorporates ten vertical micropillars of 500 µm diameter, spaced 5 mm apart. The second channel, shown in Fig. 1, has a $150\,\mu\mathrm{m} \times 150\,\mu\mathrm{m}$ square cross-section which divides into three $50\,\mu\mathrm{m} \times 50\,\mu\mathrm{m}$ square channels.

Finally, we report preliminary measurements from the first DPT Challenge (Rossi et al., June 26-28, 2025). The 1 mm-thick glass plate used to seal the Chip-in-the-Box (ChiB) challenge chip lies significantly outside the nominal optical design range of the system and introduces additional

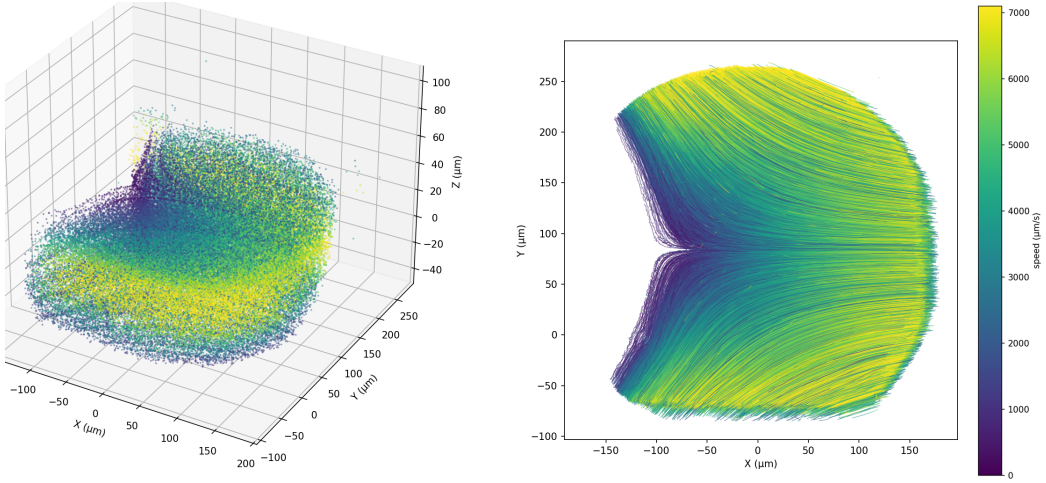


Figure 4. Particle tracks in the wake of the 500 µm pillar in the microchannel: isometric view (left) and top-down view (right). In total, there are 1 M track points, and 26 k tracks. Points are colored by speed between 0 and 7 mm/s.

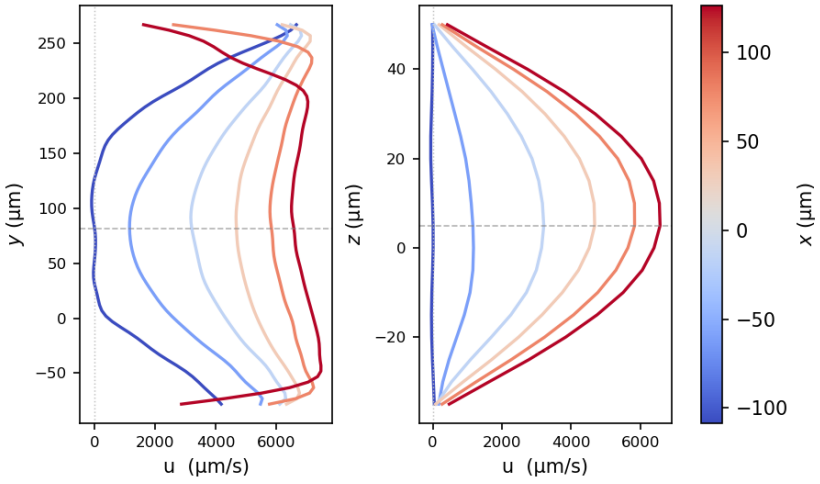


Figure 5. Developing streamwise velocity profiles along the channel centerlines in the wake of the micropillar.

aberrations and distortions that reduce tracking performance, as discussed in Sect. 2.2. Nevertheless, the results are encouraging and demonstrate the potential of this approach in challenging optical configurations.

3.1. Pillar wake

For the pillar-wake measurements, the 370 µm-wide field of view is focused on the wake of the seventh micropillar, located 40 mm downstream of the inlet. The focal plane of the imager is positioned at the channel mid-height. Particles are injected using a 1 mL syringe at a flow rate of 500 µL/min.

Figure 3 shows an instantaneous image containing the seven angular views captured by the single-

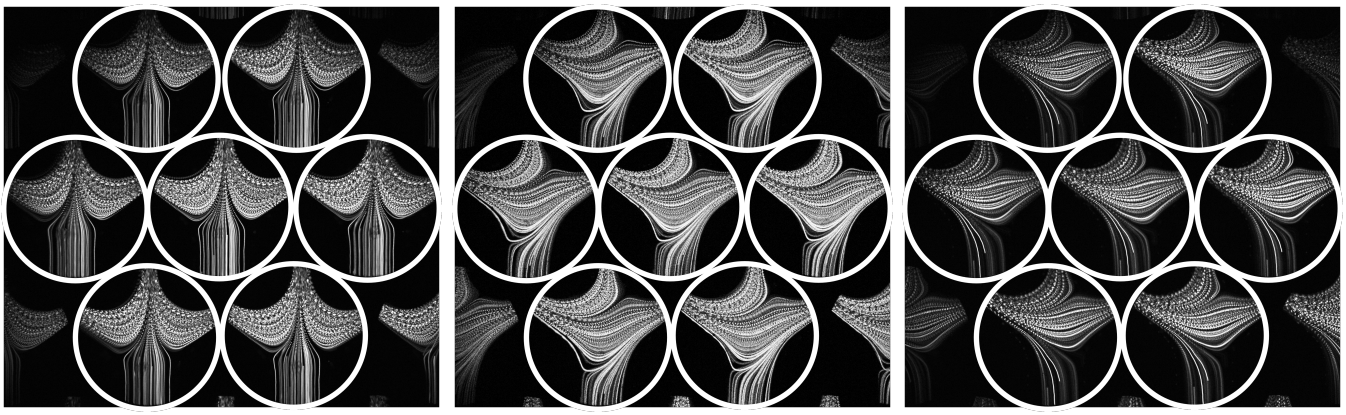


Figure 6. Streak images over 650 consecutive frames corresponding to 0.5 s for the three junction-flow cases. The background has been subtracted and the contrast has been enhanced.

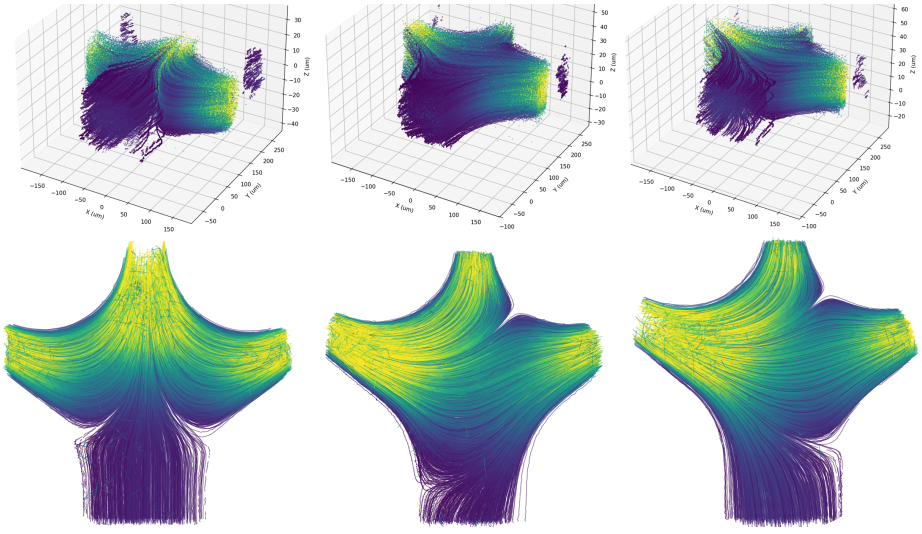


Figure 7. Particle tracks in the three junction-flow configurations: isometric view (top) and top-down view (bottom). Points are colored by speed between 0 and 22 mm/s.

camera system, together with streak images obtained by taking the intensity maximum over 130 consecutive frames, corresponding to 0.1 s. The particle image density is typically between 0.0005 and 0.001 ppp. While this density is relatively low for DPT and LPT, it will be increased in future deployments once iterative particle reconstruction is implemented in the processing algorithm.

Figure 4 shows the 26 k particle tracks obtained with 1 M track points, which align with the streak visualization in Fig. 3. Figure 5 extracts the developing streamwise velocity profile along the two symmetry planes. Eulerian velocity fields are represented using a continuous radial basis function with weights obtained from ensemble regression (Ratz & Mendez, 2024).

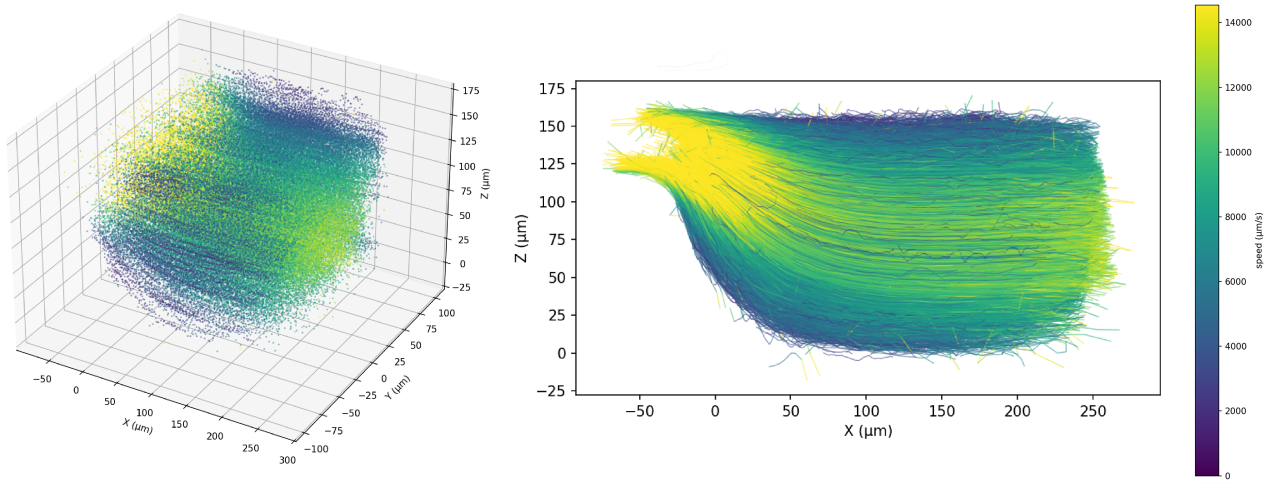


Figure 8. Particle tracks over a backward-facing step in a microchannel: isometric view (left) and side view (right). The reconstruction contains 180 k track points and 8 k tracks. Points are colored by speed between 0 and 15 mm/s.

3.2. Junction flows

The junction-flow experiments are performed in the square-channel splitter geometry. One syringe pump drives the flow in the main 150 µm channel toward the three 50 µm channels using a 5 mL syringe at flow rates of 0.5, 0, or 2.5 µL/min. A second syringe pump, connected to a 1 mL syringe and operated at 5 µL/min, drives the input shown in the second splitter unit of Fig. 1. In the first configuration, the solution is injected from the two side channels and exits through the central channel. In the two subsequent configurations, the flow is driven through the right-side and central channels and exits through the left-side channel. These cases produce different acceleration patterns and therefore provide useful tests for particle-tracking algorithms.

Figure 6 shows streak images for the three flow configurations, obtained by taking the intensity maximum over 650 consecutive frames corresponding to 0.5 s.

3.3. Backward-facing step

Test section 1 of the first DPT challenge is a backward-facing step in a rectangular microchannel. Here, we report results for the nominal 10 µL/min flow-rate condition using a 1 mL syringe. The particle concentration was three times lower than in the other cases. Figure 8 shows the measured particle tracks, and Fig. 9 extracts the developing streamwise velocity profile along the two symmetry planes.

The second condition tested for the DPT Challenge, at 300 µL/min, proved particularly challenging for the current iteration of the system because the 100 µs exposure time introduced substantial motion blur at these velocities under continuous LED illumination. Despite these limitations, the

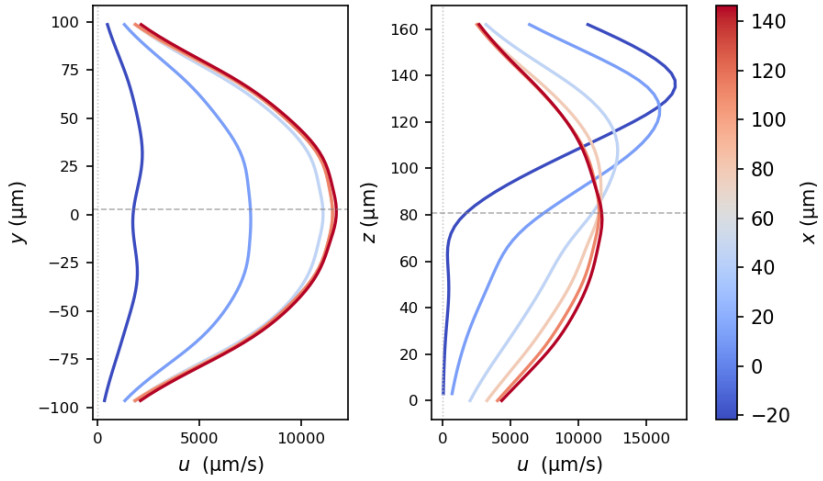


Figure 9. Developing streamwise velocity profiles past the backward-facing step

expected recirculation bubble downstream of the step was still captured.

The present processing pipeline remains fully single-pass and non-iterative. Therefore, our participation in the first DPT Challenge should be considered an early-stage demonstration. Even so, the results are encouraging and highlight the potential of this approach for future development.

4. Future work and applications

This diagnostic platform is now being extended beyond seeded-particle velocimetry toward multiphysics measurements in microchannels. The goal is to preserve the high-resolution 3D flow-tracking capability of the FIMic system while expanding the observable quantities to include biological structures, scalar fields, fluorescently labeled materials, and optically distinct interfaces. The experimentally registered PSF framework presented in Sect. 2.2 is central to this effort, as it enables calibration not only for spherical tracer particles, but also for objects and intensity features with different sizes, shapes, and emission characteristics.

One near-term application concerns microchannel flows with modified wall conditions. Microchannels are being fabricated with selectively applied hydrophilic and hydrophobic coatings to investigate their influence on near-wall flow structure, including possible slip behavior. These experiments aim to capture subtle variations in shear and particle transport near boundaries, which remain difficult to resolve with conventional imaging systems because of anisotropic resolution and limited optical access.

In parallel, we are developing experiments involving biofouling, either by flowing suspensions of cells and diatoms or by cultivating biofilms in situ under controlled conditions. These measurements aim to resolve early-stage attachment and growth dynamics together with the surrounding

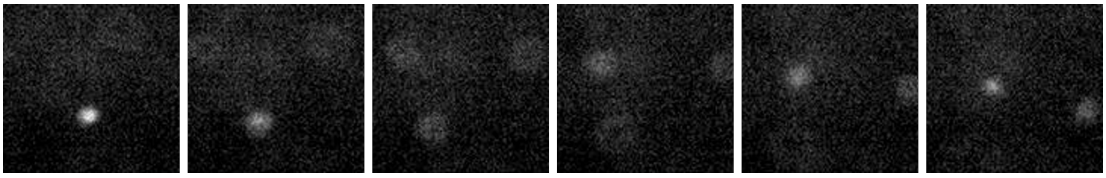


Figure 10. Central view with back-illuminated *Dunaliella* active microswimmers moving in and out of focus at 6 Hz, shown after background subtraction, intensity inversion, and contrast enhancement.

flow field. To improve biological contrast, we will explore fluorescent-stain candidates for weakly autofluorescent cells, while maintaining compatibility with live or minimally perturbed samples. We will also investigate strategies for imaging the transparent extracellular polymeric substance (EPS) matrix, either by labeling the matrix directly, embedding fluorescent particles within it, or reconstructing its overall shape as a volumetric intensity feature.

These developments will allow the system to reconstruct multiple types of physical information from a single imaging platform: Lagrangian tracer trajectories for the flow, volumetric intensity distributions for scalar or biological structures, and shape or interface features associated with cells, biofilms, or EPS matrices. This capability will support direct measurements of how biological structures modify local velocity gradients and how flow, in turn, influences growth morphology.

For cases where simultaneous fluorescence imaging of tracers and biological structures is limited by spectral overlap, weak emission, or photon budget, we will explore offset pulsed illumination strategies. One possible implementation is to combine epifluorescence illumination for particle-based flow measurements with temporally offset back-illumination for cells or biofilm structures. This would allow flow and morphology to be captured within the same optical system while reducing ambiguity between tracer fluorescence and structural contrast. We will also investigate coupling the microscope to more powerful continuous or pulsed laser sources delivered through fiber optics. Compared with the current LED-based illumination, fiber-coupled laser illumination could increase signal levels, improve exposure control, and enable shorter pulses for high-speed measurements with reduced motion blur.

The same PSF-based calibration framework also opens opportunities for studies of active microswimmers. We will use this capability to monitor the coupling between the 3D motion of microorganisms and a particle-seeded background flow, as in recently published studies (Giuliani et al., 2021; Mehmood et al., 2025; Pradipta et al., 2026). Figure 10 shows preliminary measurements of the green alga *Dunaliella* moving in and out of focus. These swimmers are slightly oblate spheroids with approximate dimensions of $7\ \mu\mathrm{m} \times 10\ \mu\mathrm{m}$.

Complementary to trajectory-based STB reconstructions, we are developing intensity reconstructions to capture volumetric scalar fields from broad fluorescence emissions, such as dye-injected or molecularly tagged flows (Huck et al., 2025; Halder et al., January 12-16, 2026). RLD and neural radiance fields provide a complementary perspective in regions with high particle concentra-

tion, diffuse tracers, or extended biological structures where individual particle tracking becomes unreliable. Combined with STB and data-assimilation techniques currently under development, these reconstructions have the potential to enable temporally and spatially resolved Eulerian, Lagrangian, and intensity-based features to be extracted from a single acquisition.

5. Conclusions

This work demonstrates the continued development of high-speed Fourier integral, or light-field, microscopy as a compact single-camera platform for 4D particle tracking in microchannels. By capturing seven angular views on a single 6K high-speed sensor, the FIMic system provides volumetric access without the alignment complexity of multi-camera tomographic or stereoscopic arrangements. In its initial implementation, the system achieved nearly isotropic particle-localization uncertainty below 0.3 µm, with lateral uncertainties below 0.1 µm, and supported time-resolved measurements at 1300 Hz streamed directly to disk over 20 s acquisitions.

The present work substantially expands this capability by incorporating experimentally registered defocused PSFs and view-wise neural-network particle detection. These improvements extend the reconstructed depth from the original 50 µm range to more than 160 µm while maintaining a 370 µm-wide field of view. The resulting measurement volume and acquisition rate enable dense, time-resolved Lagrangian descriptions of microchannel flows, as demonstrated in pillar wakes, junction-flow configurations, and a backward-facing step geometry. Across these cases, the system reconstructs large ensembles of 3D tracks, including datasets with up to 1 M track points and 26 k trajectories in the pillar-wake flow.

The results also show that the method can operate in challenging optical configurations, including microchannels with thicker sealing layers, as chosen for the first DPT Challenge. The present processing framework remains single-pass and non-iterative, and therefore is less mature than single-camera DPT approaches. Work is ongoing to take full advantage of the complementary nature of the high-resolution plenoptic imaging, with experimentally calibrated PSFs and multi-view particle reconstruction.

Looking forward, the same framework provides a path toward multiphysics measurements. Future developments will focus on increasing particle image density, improving temporal linking and iterative reconstruction, and combining Lagrangian particle tracking with intensity-based reconstructions. This will allow the system to move beyond particle-based velocimetry and toward coupled measurements of near-wall transport, scalar fields, biofilm growth, active microswimmers, and evolving biological or material interfaces. While the present applications focus on microscale flows, the underlying approach may also be extended to other wall-bounded turbulent flows where compact, high-resolution volumetric imaging is often required.

Acknowledgments

This work is supported by ONR grants N00014-23-2-2001, N00014-25-1-2243, and N00014-26-1-2106 managed by Dr. Yin-Lu (Julie) Young. M. J. Yamakaitis is a DOD SMART scholar. We are grateful to Drs. C. Cierpka, S. Sachs, and M. Rossi for organizing the first DPT Challenge and for giving us the opportunity to participate despite our late entry.

References

Barnkob, R., Kähler, C. J., & Rossi, M. (2015). General defocusing particle tracking. *Lab on a Chip*, *15*(17), 3556–3560. doi: 10.1039/C5LC00562K

Cierpka, C., & Kähler, C. J. (2012). Particle imaging techniques for volumetric three-component (3D3C) velocity measurements in microfluidics. *Journal of visualization*, *15*(1), 1–31. doi: 10.1007/s12650-011-0107-9

Etminan, A., Muzychka, Y. S., Pope, K., & Nyantekyi-Kwakye, B. (2022). Flow visualization: state-of-the-art development of micro-particle image velocimetry. *Measurement Science and Technology*, *33*(9), 092002. doi: 10.1088/1361-6501/ac75b0

Fort, C., Solomon, H., Capanna, R., Wang, S., Li, Z., & Bardet, P. (July 8-11, 2024). Fourier light-field microscope for micro tomo-PTV in a cross-junction microfluidic channel. In *Proceedings of the 21st international symposium on applications of laser and imaging techniques to fluid mechanics, lisbon, portugal.* doi: 10.55037/lxlaser.21st.195

Fort, C., Yamakaitis, M., & Bardet, P. (June 26-28, 2025). Progress on microscopic single-camera 3D Lagrangian particle tracking. In *Proceedings of the 16th international symposium on particle image velocimetry, tokyo, japan.*

Giardino, J., Hertzberg, J., & Bradley, E. (2008). A calibration procedure for millimeter-scale stereomicroscopic particle image velocimetry. *Experiments in fluids*, *45*, 1037–1045. doi: 10.1007/s00348-008-0525-1

Giuliani, N., Rossi, M., Noselli, G., & DeSimone, A. (2021). How *Euglena gracilis* swims: flow field reconstruction and analysis. *Physical Review E*, *103*(2), 023102. doi: 10.1103/PhysRevE.103.023102

Godbersen, P., Schanz, D., & Schröder, A. (2024). Peak-cnn: improved particle image localization using single-stage cnns. *Experiments in Fluids*, *65*(10), 153.

Halder, S., Yamakaitis, M., Sapkota, B., **Fort**, t., Bardet, P., & Thurow, B. (January 12-16, 2026). Development of tomographic reconstruction method for MTV using neural radiance fields. In *Proceedings of aiaa scitech 2026 forum, orlando, fl* (p. 2100). doi: 10.2514/6.2026-2100

Hao, K., Hans, A., Vlachos, P., & Bilionis, I. (2024). Unbalanced optimal transport for stochastic particle tracking. *arXiv preprint arXiv:2407.04583*.

He, Q., Willman, C., Stone, R., & Williams, B. A. (2023). Inexpensive multi-plane particle image velocimetry based on defocusing: Proof of concept on two-component measurement. *Physics of Fluids*, *35*(6). doi: 10.1063/5.0151952

Huck, P., Yamakaitis, M., Fort, C., & Bardet, P. (2025). Near-wall volumetric molecular tagging velocimetry with a Fourier integral microscope. *Experiments in Fluids*, *66*(152). doi: 10.1007/s00348-025-04078-x

Kim, H., Groe, S., Elsinga, G. E., & Westerweel, J. (2011). Full 3D-3C velocity measurement inside a liquid immersion droplet. *Experiments in Fluids*, *51*(2), 395–405. doi: 10.1007/s00348-011-1053-y

Klinner, J., & Willert, C. (2022). Feasibility of multi-aperture μPTV for wall shear stress measurements. In *Proceedings of the 20th international symposium on applications of laser and imaging techniques to fluid mechanics* (p. 921-946). Lisbon, Portugal. doi: 10.55037/lxlaser.20th.167

Liang, J., Cai, S., Xu, C., Chen, T., & Chu, J. (2021). Deepptv: Particle tracking velocimetry for complex flow motion via deep neural networks. *IEEE Transactions on Instrumentation and Measurement*, *71*, 1–16.

Lindken, R., Westerweel, J., & Wieneke, B. (2006). Stereoscopic micro particle image velocimetry. *Experiments in Fluids*, *41*(2), 161–171. doi: 10.1007/s00348-006-0154-5

Mallery, K., Shao, S., & Hong, J. (2020). Dense particle tracking using a learned predictive model. *Experiments in Fluids*, *61*(10), 223.

Mehmood, J., Muller, K., Kumar, S., Buchner, A.-J., & Tam, D. (2025). Three-dimensional tracking of microswimmer suspensions. *Experiments in Fluids*, *66*(4), 81. doi: 10.1007/s00348-025-04002-3

Mercier, B., Thomas, L., Tremblais, B., & David, L. (2024). A robust pairing method for two-pulse particle tracking velocimetry based on coherent point drift. *Measurement Science and Technology*, *35*(6), 065301.

Novara, M., Schanz, D., & Schröder, A. (2023). Two-pulse 3d particle tracking with shake-the-box. *Experiments in Fluids*, *64*(5), 93.

Oishi, M., Kinoshita, H., Fujii, T., & Oshima, M. (2011). Simultaneous measurement of internal and surrounding flows of a moving droplet using multicolour confocal micro-particle image velocimetry (micro-PIV). *Measurement Science and Technology*, *22*(10), 105401. doi: 10.1088/0957-0233/22/10/105401

Ooms, T., Lindken, R., & Westerweel, J. (2009). Digital holographic microscopy applied to measurement of a flow in a T-shaped micromixer. *Experiments in Fluids*, *47*, 941–955. doi: 10.1007/s00348-009-0683-9

Ouellette, N. T., Xu, H., & Bodenschatz, E. (2006). A quantitative study of three-dimensional lagrangian particle tracking algorithms. *Experiments in Fluids*, *40*(2), 301–313.

Park, J. S., Choi, C. K., & D Kihm, K. (2004). Optically sliced micro-PIV using confocal laser scanning microscopy (CLSM). *Experiments in Fluids*, *37*, 105–119. doi: 10.1007/s00348-004-0790-6

Pereira, F., Lu, J., Castano-Graff, E., & Gharib, M. (2007). Microscale 3D flow mapping with μDDPIV. *Experiments in fluids*, *42*, 589–599. doi: 10.1007/s00348-007-0267-5

Pradipta, G., Lee, W., Tran, V., Welch, K., Sankar, S. K., Kim, Y., … others (2026). Seeing new depths: Three-dimensional flow of a free-swimming alga. *Physical Review X*, *16*(2), 021019. doi: 10.1103/2rr3-lbrn

Ratz, M., & Mendez, M. A. (2024). A meshless and binless approach to compute statistics in 3d ensemble ptv. *Experiments in Fluids*, *65*(9), 142.

Rossi, M., Sachs, S., & Cierpka, C. (June 26-28, 2025). First Defocus Particle Tracking challenge: Chip-in-the-Box and multi-flavor datasets. In *Proceedings of the 16th international symposium on particle image velocimetry, tokyo, japan.*

Schanz, D., Gesemann, S., & Schröder, A. (2016). Shake-the-box: Lagrangian particle tracking at high particle image densities. *Experiments in fluids*, *57*(5), 70.

Sheng, J., Malkiel, E., & Katz, J. (2006). Digital holographic microscope for measuring three-dimensional particle distributions and motions. *Applied optics*, *45*(16), 3893–3901. doi: 10.1364/AO.45.003893

Winer, M. H., Ahmadi, A., & Cheung, K. C. (2014). Application of a three-dimensional (3D) particle tracking method to microfluidic particle focusing. *Lab on a Chip*, *14*(8), 1443–1451. doi: 10.1039/C3LC51352A

Yoon, S. Y., & Kim, K. C. (2006). 3D particle position and 3D velocity field measurement in a microvolume via the defocusing concept. *Measurement Science and Technology*, *17*(11), 2897. doi: 10.1088/0957-0233/17/11/006